Early-onset of pressure-induced metallization in iron-doped multilayered molybdenum disulfide ⊘

Chih-Ming Lin ✉ ⓘ ; Der-Yuh Lin ⓘ ; Jenh-Yih Juang ⓘ ; Tony Huang; Dong-Zhou Zhang ⓘ ; Yi-Jia Tsai ⓘ ; Sheng-Rui Jian ✉ ⓘ ; Joon-Seok Kim ✉ ⓘ ; Jung-Fu Lin ⓘ

Check for updates

View Online   Export Citation

Early-onset of pressure-induced metallization in iron-doped multilayered molybdenum disulfide

View Online   Export Citation   CrossMark

Chih-Ming Lin,[1,a)] Der-Yuh Lin,[2] Jenh-Yih Juang,[3] Tony Huang,[4] Dong-Zhou Zhang,[5] Yi-Jia Tsai,[1] Sheng-Rui Jian,[6,7,a)] Joon-Seok Kim,[8,a)] and Jung-Fu Lin[9]

AFFILIATIONS

[1]Department of Physics, National Tsing Hua University, Hsinchu 30013, Taiwan

[2]Department of Electronic Engineering, National Changhua University of Education, Changhua 500, Taiwan

[3]Department of Electrophysics, National Yang Ming Chiao Tung University, Hsinchu 300, Taiwan

[4]Department of Earth Sciences, National Cheng Kung University, Tainan 701, Taiwan

[5]GeoSoilEnviroCARS, Argonne National Laboratory, Argonne, Illinois 60439, USA

[6]Department of Materials Science and Engineering, I-Shou University, Kaohsiung 840, Taiwan

[7]Department of Fragrance and Cosmetic Science, College of Pharmacy, Kaohsiung Medical University, 100 Shi-Chuan 1st Road, Kaohsiung 80708, Taiwan

[8]Department of Electrical and Computer Engineering, The University of Texas at Austin, Austin, Texas 78758, USA

[9]Department of Earth and Planetary Sciences, Jackson School of Geosciences, The University of Texas at Austin, Austin, Texas 78712, USA

[a)]Authors to whom correspondence should be addressed: cm_lin@phys.nthu.edu.tw. **Tel.:** (886) 3-5742521. **Fax:** (886) 3-55723052; srjian@isu.edu.tw; and jskhan87@gmail.com

ABSTRACT

Chemical doping-induced magnetism in semiconducting transition metal dichalcogenides (TMDC) can have significant implications in electrically controlled spintronics. In addition, strain engineering of the layered structures of TMDCs can further allow for tuning the interlayer van der Waals (vdW) bonds and controlling their electronic properties. Of particular interest are the effects of Fe doping coupled with strain tuning on the vdW bonds and associated electronic properties of Fe:MoS_2. Here, we have investigated compressive strain tuning effects on the structural and vibrational properties of Fe:MoS_2 using *in situ* angle-dispersive x-ray diffraction and Raman scattering spectroscopy at quasi-hydrostatic pressures up to 25.0(1) GPa. Our results indicate that Fe:MoS_2 undergoes isostructural electronic transitions similar to those in pristine MoS_2, but at significantly lower pressures. Sudden changes in the microscopic strain, Raman peak splitting, and phonon softening are observed at the transition pressures, suggesting that the structural instability introduced by the Fe dopants is responsible for the early onset of the transitions. The significant effects of Fe dopants on the interlayer vdW bonding, as well as the structural and phononic properties under compressive strain indicate a strategy for modulating the electronic and ferromagnetic properties of TMDCs.

Published under an exclusive license by AIP Publishing. https://doi.org/10.1063/5.0202113

Molybdenum disulfide (MoS_2) is a promising candidate for next generation spintronic, electronic, and optoelectronic applications[1–4] due to its excellent electronic mobility reaching $\sim10^3$ cm²/V·s and layer-dependent sizeable bandgap.[3–6] The absence of inversion symmetry in MoS_2 further leads to strong spin-valley coupling and opens the opportunities for valley-based spintronics applications. One way of manipulating the spin-polarized charge carriers is to incorporate magnetism into MoS_2 by chemical doping, such as iron, to form diluted magnetic semiconductor (DMS). Indeed, Fe-doped MoS_2 (Fe:MoS_2) has been reported to exhibit room-temperature ferromagnetism

(RTFM) down to the monolayer limit.[7,8] Density functional theory (DFT) calculations further indicate that Fe-doping introduces in-gap states and shifts the Fermi level close to the conduction band minimum, giving rise to the observed RTFM.[7,8] By incorporating the magnetism degree of freedom with the well-studied exotic material properties of MoS_2, the Fe:MoS_2 will allow for various engineering approaches to tune the magnetism. For example, gate-modulation of electronic transport and exciton emission,[9] dielectric encapsulation-induced bandgap modulation,[10] ultrafast charge separation in van der Waals (vdW) heterostructure,[11] and moiré superlattice that gives rise

to ferroelectricity[12] could all encompass additional spin-dependence effects with Fe:MoS$_2$ in place of MoS$_2$.

Alternatively, strain engineering is very effective in tuning the van der Waals (vdW) bonds and thus the electronic properties of the transition-metal dichalcogenides (TMDCs).[13] Theoretical[14–17] and experimental[18–20] studies have shown that bulk MoS$_2$ undergoes pressure-induced semiconducting-to-metallic transition due to the reduced interlayer spacing and enhanced sulfur–sulfur (S-S) interaction. The pressure-induced vdW bonding modulation is even more effective in monolayer TMDCs, wherein the lack of interlayer interaction enhances bandgap opening due to hydrostatic compression.[13,21] Structurally, no first-order structural phase transition was reported for the pristine MoS$_2$ (P-MoS$_2$) up to ~60 GPa, except for the 2H$_c$-to-2H$_a$ isostructural transition, which has been theoretically argued to proceed through the sliding of the layers in the unit cell without altering the crystal space group D_{6h}^4.[18–20] However, the proposed scenario remains unsettled experimentally.[18,19] López-Suárez et al.[22] pointed out that application of compressive strain can result in out-of-plane deformation and trigger the electronic transitions in few-layer MoS$_2$. Cheng et al.[23] reported that the pressure-induced 2H$_c$-to-2H$_a$ isostructural transition in MoS$_2$ is thickness-dependent, indicating the importance of vdW interaction in modulating the structural and electronic properties. In view of the lack of studies on how chemical doping affects the pressure-induced structural transition in multilayer MoS$_2$, it is imperative to further delineate what happens when both strain and extrinsic electronic states are introduced simultaneously. In this study, systematic in situ angle-dispersive x-ray diffraction (ADXRD) and Raman scattering measurements in a diamond anvil cell on multilayered P-MoS$_2$ and Fe:MoS$_2$ were conducted to reveal the effects of Fe-doping with pressures up to 24.8(2) GPa.[7]

Sample preparation and experimental methods are described in the supplementary material. Briefly, bulk MoS$_2$ and Fe:MoS$_2$ crystals were synthesized using CVT method, which were then grounded to a powder before being loaded and pressurized in a diamond anvil cell. Note that our specimen, denoted as multilayer, still maintains the vdW layered structure (supplementary material, Figs. 8–11), and is of thickness beyond where the structural, electronic, and phononic properties lose their layer-dependency. Inductively coupled plasma optical

emission spectrometer (ICP-OES) results indicate that the Fe concentration is approximately 0.21 at. % (Fig. S1), which is below the reported solubility limit of 0.3–0.5 at. % governed primarily by ionic radii mismatch and structural difference between MoS$_2$ (2H$_c$ trigonal) and FeS$_2$ (cubic).[24] Raman spectra of Fe:MoS$_2$ show no additional peaks or features compared to P-MoS$_2$, suggesting that the doping does not cause major adjustment to the lattice vibration modes [Fig. 1(a)]. The in-plane E$^1_{2g}$ peak in Fe:MoS$_2$ shows slight blue-shift compared to P-MoS$_2$, indicating a smaller lattice constant in the in-plane direction. The lattice parameters and the atomic volume of Fe:MoS$_2$ extracted from ambient pressure XRD [Fig. 1(b)] are $a = b = 3.1591(1)$ Å, $c = 12.3079(6)$ Å, and V/Z = 53.187(3) Å^3, respectively. These values are slightly smaller than the values of $a = b = 3.1680(1)$ Å, $c = 12.3220(1)$ Å, and V/Z = 53.550(1) Å for P-MoS$_2$ (ICSD #95570), likely due to the smaller ionic radius of Fe^{4+} (0.5850 Å) compared to that of Mo^{4+} (0.6500 Å).[25]

In situ ADXRD spectra of Fe:MoS$_2$ obtained from a compression run up to 19.7(1) GPa with that of the decompressed sample are shown in Fig. 2(a). Evolution of five representative diffraction peaks corresponding to (002), (100), (101), (102), and (103) crystallographic planes of 2H$_c$ phase are labeled accordingly. All the Bragg peaks shift to larger angles, indicating the progressive lattice shrinkage in Fe:MoS$_2$. The ADXRD patterns show no trace of iron or iron oxide clusters or signs of newly formed phases up to 19.7(1) GPa, suggesting a homogeneous doping and absence of pressure-induced structural phase transition. The decompressed pattern shows that Fe:MoS$_2$ appeared to have completely recovered back to the original hexagonal crystal structure.

Figure 2(b) shows the pressure-dependence of the interplanar distance (d_{hkl}) of {002} and {100} planes for Fe:MoS$_2$ (additional interplanar distances are included in Fig. S2). Although along the compression course all the diffraction peaks can be refined to crystallographic planes of 2H$_c$-structured MoS$_2$ and no new diffraction peak is observed up to 19.7(1) GPa, noticeable discontinuities in d_{hkl} decrease rate are observed at pressures of 6.5(1) and 13.5(1) GPa, respectively. Here, we define three pressure zones according to the d_{hkl} decreasing rate, namely zone I [0–6.5(1) GPa], zone II [6.5(1)–13.5(1) GPa], and zone III [13.5(1)–19.7(1) GPa]. Linear compressibility
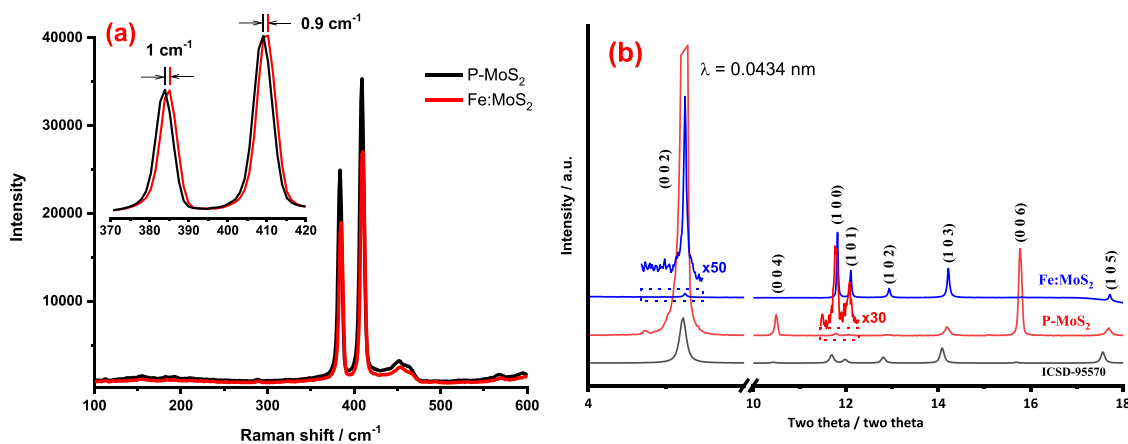
FIG. 1. (a) Raman spectra of Fe:MoS$_2$ and P-MoS$_2$. The inset shows normalized spectra of E$_{2g}$ and A$_{1g}$ peaks. (b) X-ray diffraction spectra of Fe:MoS$_2$ and P-MoS$_2$. A reference pattern from ICSD-95570 is plotted for comparison.
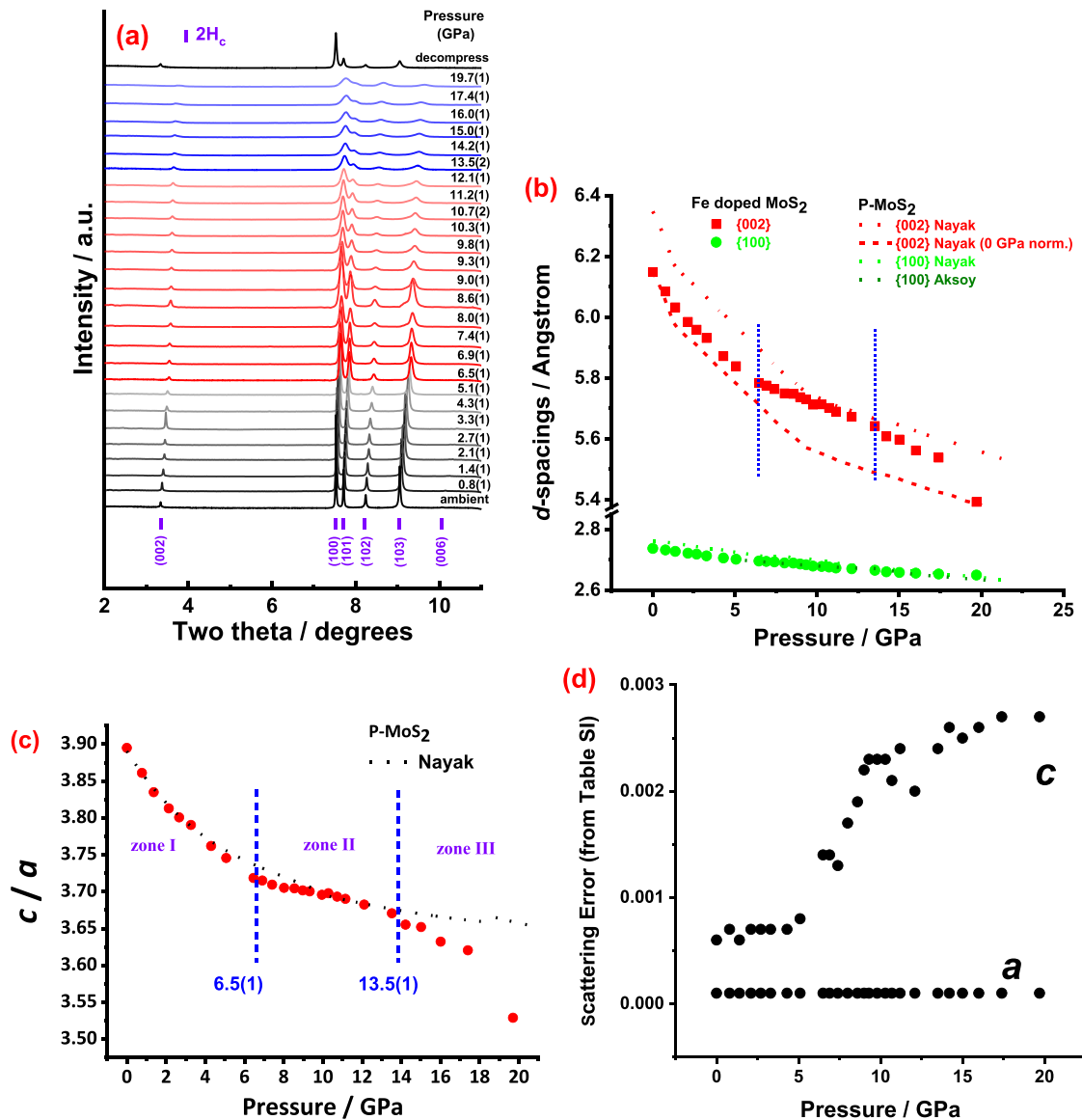
FIG. 2. (a) ADXRD spectra of multilayered Fe:MoS$_2$ at pressures up to 19.9(1) GPa. The spectrum from decompressed sample is plotted at the top for comparison. (b) Pressure dependence of the d_{002} and d_{100} spacings in multilayered Fe:MoS$_2$ at room temperature (Symbols). Lines indicate reported data of pristine MoS$_2$ from the literature. (c) Pressure dependence of c/a ratio of Fe:MoS$_2$ (symbols) and reported values of P-MoS$_2$ (line). Three pressure zones are identified in panels b and c. (d) XRD peak fitting errors, for a- and c-lattice parameters, resulting from inhomogeneous broadening of XRD peaks as a function of pressure.

$Kd_{hkl} = -(1/d_{hkl})[d(d_{hkl})/dP]_T$ is extracted from the pressure-dependent d_{hkl} for the three pressure zones and the results are listed in Table I. From the pressure-dependent c/a ratio displayed in Fig. 2(c) and the compressibility values shown in Table I, it is evident that the average compressibility along the c-axis is larger than that along the a- or b-axis in all three pressure zones, presumably due to the vdW interlayer bonding of the layered structure. The anisotropy is particularly strong in zone I, suggesting that in this pressure range, the compression affects the interlayer distance more effectively. With further increasing the pressure to zone II, the compressibility along each individual crystallographic orientation becomes more isotropic, implying that the strength of interlayer bonding becomes comparable to that of intralayer covalent bonding. The normalized decrease rate for the c-parameter is approximately four times of that of the a-parameter in zone I, whereas the ratio reduces to about 2 in zone II, implying that the enhanced S-S interaction may be responsible for reducing the compressibility along the c-axis. The compression becomes anisotropic again in zone III, in which the d_{002} spacing experiences sudden collapse at ~19.5 GPa [Figs. 2(b) and 2(c)]. Similar pressure-dependence discontinuities appear in the volume change as shown in Fig. S3.

TABLE I. Linear incompressibility of Fe:MoS$_2$ at high pressure.

	$K_{d_{002}}$ (GPa^{-1})	$K_{d_{100}}$ (GPa^{-1})
Zone I ambient to 6.5(1) GPa	1.291×10^{-2}	3.106×10^{-3}
Zone II 6.5(1)–13.5(1) GPa	2.836×10^{-3}	2.263×10^{-3}
Zone III 13.5(1)–19.7 GPa	6.682×10^{-3}	4.803×10^{-3}

The values of volume compressibility $K_V = -(1/V_0)[dV/dP]_T$ extracted for each pressure zones are $\approx 1.91 \times 10^{-2}$, 8.09×10^{-3}, and 8.23×10^{-3} GPa^{-1} for zones I, II, and III, respectively.

The evolution of Fe:MoS$_2$ d_{002} compression is particularly intriguing when compared with those of P-MoS$_2$ [lines in Fig. 2(b)], where the change in d_{002} compression slope (i.e., Kd_{002}) occurs at $\sim 8.0(1)$ GPa and was attributed to an isostructural electronic phase transition from semiconductor to an intermediate state.[18,19] The behavior of compression slope in Fe:MoS$_2$ closely resembles that of P-MoS$_2$ and thus may also be attributed to the similar isostructural electronic transition, only with a significantly lower onset pressure [$\sim 6.5(1)$ GPa]. The early onset of electronic transition is likely due to the smaller interplanar spacing of Fe:MoS$_2$ at ambient condition (6.1481 Å) than that of P-MoS$_2$ (6.2000 Å).[26] It is worth mentioning that the K_c and K_a of Fe:MoS$_2$ in zone I are slightly less than those of pristine 2H$_c$ MoS$_2$ ($K_c = 16.4 \pm 0.3$ and $K_a = 3.4 \pm 0.1$ GPa^{-1}, respectively,) at pressure below 5 GPa,[27] suggesting that in the low pressure regime, the a- and c-axis of Fe:MoS$_2$ is less compressible than the P-MoS$_2$. Considering that the magnitudes of Pauling's electronegativity for S, Mo, and Fe are 2.58, 2.16, and 1.83, respectively,[25] significantly more charge transfer from Fe to S is expected than from Mo. As a result, stronger ionic bonding is anticipated in Fe:MoS$_2$ than in MoS$_2$, which could explain the a- and c-axis being smaller and less compressible than those in P-MoS$_2$ in the low pressure regime. Moreover, Connell et al.[28] argued that the S atoms at the corners of the trigonal prisms with saturated 3s subshells are responsible for the interlayer vdW force. Thus, the introduction of Fe not only shortens the interlayer spacing but also enhances the S-S interaction.[20] Increase in $Kd002$ was also reported in P-MoS$_2$ at ~ 19 GPa and was attributed to the electronic transition to metallic state. However, the collapse of d_{002} [Fig. 2(b)] was not reported in P-MoS$_2$ at the intermediate-to-metallic transition, implying that the collapse can be linked to the doping-induced structural disturbance but not to the electronic transition. Little discrepancy was observed for d_{100} compression between Fe-doped and undoped MoS$_2$.

One possible reason for the early onset of the pressure-induced isostructural electronic transition of Fe:MoS$_2$ could be the reduced crystal ordering caused by iron doping, which, in turn, reduces the stability of the 2H$_c$ crystal structure. Similar change was observed in Fe-doped zinc blende InP, wherein the hybridization of iron 3d orbitals and phosphide p orbitals reduced the stability of InP lattice and triggered an early pressure-induced phase transition.[29] In the present case of Fe:MoS$_2$, the hybridization between the iron 3d orbitals and the sulfur 3p orbitals tends to distort the lattice structure of multilayered Fe:MoS$_2$ (Ref. 28) and, hence, will likely reduce the onset pressure of the electronic structure transition associated with the pressure-induced lattice distortion.[19] In addition, the ionic size difference between Fe^{4+} (0.5850 Å) and Mo^{4+} (0.6500 Å)[25] is also expected to result in local

lattice strain, contributing to the lowering of the transition pressure. Such structural effects, in combination with the in-gap states introduced by Fe-doping[8] that will promote metallization, can be attributed as the main mechanisms for the early onset of electronic transitions in Fe:MoS$_2$.[19,20] Alternatively, the random substitution of Mo by Fe could lead to a landscape of varying local micro-strains due to the differences in the ionic size and the associated Mo–S and Fe–S bond lengths.[30] As can be seen from Table SI and Fig. 2(d), the fitted c-axis parameters from the XRD spectra show much larger scattering errors (indicated by the number in the parenthesis) than that of the a-axis. More intriguingly, scattering error for the c-axis parameters show sudden changes when plotted as a function of pressure, i.e., abrupt increase after $\sim 5.0(1)$ GPa. Such increase in fitting error is reportedly linked to pressure-induced enhancement in the local micro-strain and variations of interlayer vdW interactions.[31] Layer-dependence of the transition pressures are suggested for future works, which could further enlighten the role of vdW interactions in Fe:MoS$_2$.

Raman spectroscopy is an effective and powerful method for detecting minute changes in the lattice vibration as well as electronic phase transitions.[32] Figure S2 shows the typical Raman spectrum obtained at ambient conditions, which indicates that 28 peaks can be identified by Lorentzian curves, consistent with previously reported experimental results for bulk MoS$_2$ (Refs. 33–37) and Fe-doped MoS$_2$ films.[38] The assignment of each Raman peak position and the proposed symmetry assignment, compared to those of P-MoS$_2$ from the literature, are presented in Table SII. It is noteworthy that both in-plane E$_{2g}^1$(Γ) and out-of-plane A$_{1g}$(Γ) frequencies of Fe:MoS$_2$ are slightly higher than those of P-MoS$_2$, in good agreement with the smaller lattice parameters.

With increasing pressure, all Raman modes shift progressively toward higher frequencies, and many of them broadened and eventually disappeared. Figure 3(a) shows the Raman spectra of Fe:MoS$_2$ at representative pressures. As shown in Fig. 3(b) and Fig. S4, deconvolution of Raman spectra with Lorentzian curves allowed identification of 13 peaks in pressure zone I. At 6.4(1) GPa, E$_{2g}^1$(Γ) and A$_{1g}$(Γ) modes become degenerate and show clear peak splitting into two peaks at 384.26 and 392.71 cm^{-1}, and 423.08 and 430.67 cm^{-1}, respectively, presumably due to the pressure-induced symmetry breaking of the crystal [Fig. 3(a); red curve].[39,40] Also, all other modes exhibit slight softening (red-shift). These anomalies at 6.4(1) GPa coincide with the transition from zone I to zone II, determined earlier from XRD analyses. The phonon softening (PS) coinciding with the phase transition is similar to the pressure-induced electronic topological transition (ETT) observed in pnictogen chalcogenide crystals,[32,41] inferring that the changes in lattice compression is related to the electronic transition in Fe:MoS$_2$, as well. Similar to the XRD analysis, no signs of the first-order phase transition were observed before and after this transition pressure. It is notable that similar peak splitting and PS were also observed in strained monolayer and bilayer MoS$_2$ (Ref. 39) and in Zn$_{0.84}$Fe$_{0.16}$Se dilute magnetic semiconductor (DMS) under high pressure.[42]

As the pressure is further increased to 12.5(2) GPa, all visible modes exhibit blue-shift with the exception of nearly unchanging A$_{1g}$(M)-ZA(M) and E$_{1u}$(M)-TA(M) modes. This suggests accelerated blue-shifts of the transverse [TA(M)] and acoustic [ZA(M)] phonons from the vicinity of the high-symmetry M point of the Fe:MoS$_2$ Brillouin zone.[36] As the pressure reaches 13.2(2) GPa, the transition
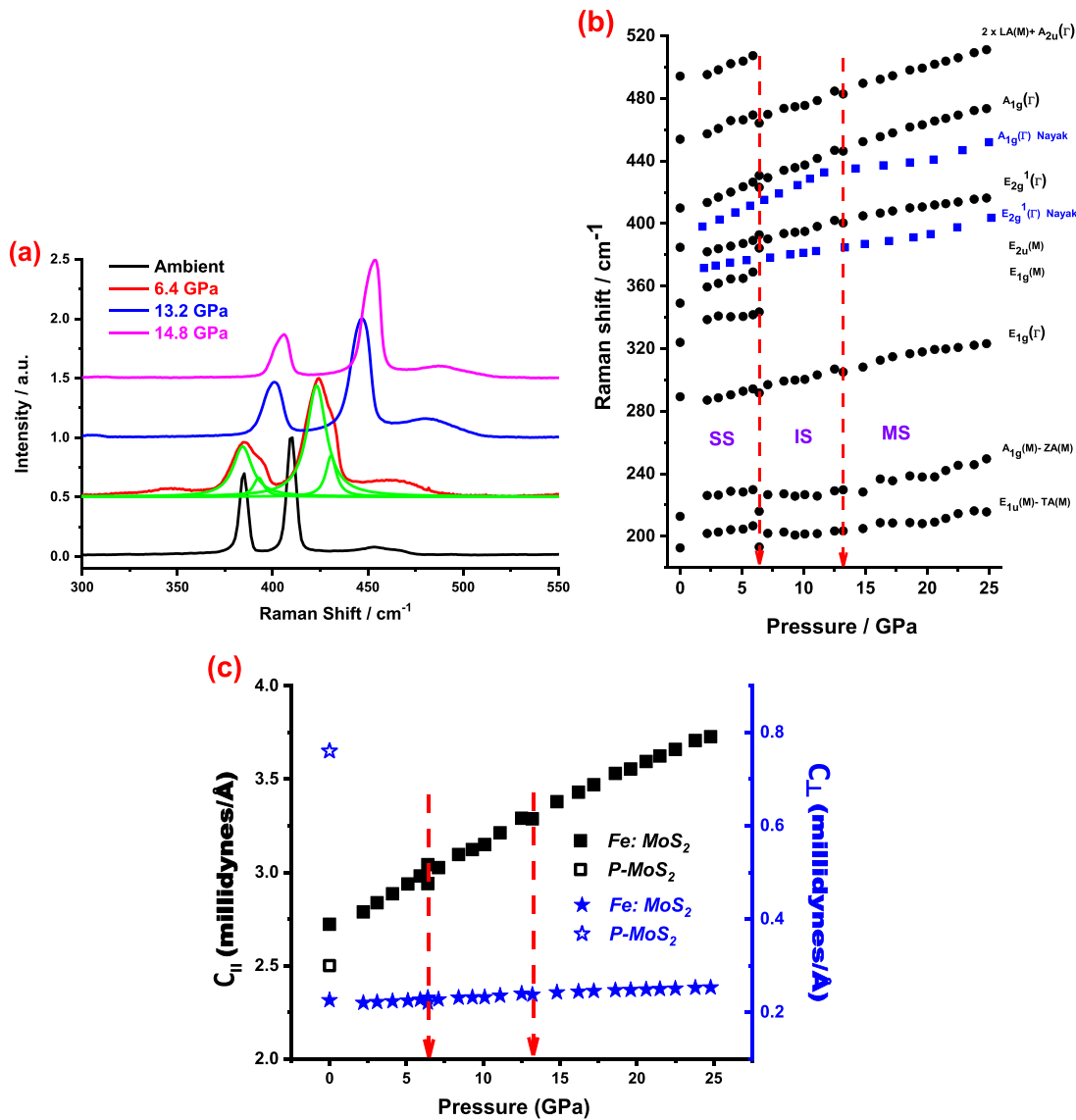
FIG. 3. (a) Raman spectra of Fe:MoS$_2$ at representative pressures. The spectrum at 6.4 GPa is fitted with multiple Lorentzian functions, showing signs of peak splitting. (b) Raman peak positions as functions of pressures. Blue symbols are the reported peak positions of P-MoS$_2$. (c) In-plane (C$_{||}$) and out-of-plane (C$_\perp$) compressive forces as a function of pressure.

pressure from zones II to III, all observable modes show slight soft-ening. The apparent PS prior to metallization and progressive hard-ening afterward have also been reported by Nayak *et al.*[19] The pressures where the peak splitting and PS occurs are in excellent agreement with ADXRD results, thus validating the assignments of zones I, II, and III according to electronic transitions. More impor-tantly, the coincidence of PS and electronic phase transition further implies the interaction between the phonons and electrons originat-ing from the inter-valence charge transfer accelerated by Fe-doping, which has been reported to play an important role in causing struc-tural distortion.[39] In fact, a plethora of layer structured materials, such as FePO$_4$, VO$_2$, and many DMSs, had been found to display a

similar electronic intermediate state accompanying the PS behavior while undergoing a transition from a semiconducting to a metallic state.[42–44]

To further reveal the relevance of the Raman shifts and structural parameters under pressure, the Grüneisen parameters (γ) of Fe:MoS$_2$ E$_{2g}^1$(Γ) and A$_{1g}$(Γ) modes in three pressure zones are extracted and listed in Table SIII. The γ values in lower pressure range are similar to those of P-MoS$_2$ [0.21 for E$_{2g}^1$(Γ) and 0.42 for A$_{1g}$(Γ)].[45] Interestingly, the γ values for both E$_{2g}^1$(Γ) and A$_{1g}$(Γ) modes are the largest in zone II, in agreement with the lattice parameter compression in Fig. 2(b), suggesting that the atomic compression is the most nonlinear in the intermediate electronic phase (zone II).

Other informative parameters to be derived from the Raman spectroscopy is the variation of the out-of-plane ($C_\perp$) and in-plane ($C_\parallel$) compressive force constants with pressure, which can be described by a linear-chain model.[33] According to the Wieting's model of equations (S5) and (S6), Fig. 3(c) shows the pressure dependence of $C_\parallel$ and $C_\perp$ (solid symbols) together with respective values at ambient-pressure (open symbols) for multilayered Fe:MoS$_2$. It is clear that, at ambient pressure, the $C_\perp$ value for Fe:MoS$_2$ ($C_\perp = 0.23$ millidynes/Angstrom; md/Å) is significantly smaller than that of P-MoS$_2$ ($C_\perp \approx 0.76$ md/Å), while the respective values of $C_\parallel$ are comparable ($C_\parallel = 2.72$ md/Å vs $C_\parallel \approx 2.50$ md/Å), indicating that iron-doping has induced significant softening of the out-of-plane vibrating mode [A$_{1g}(\Gamma)$], while the in-plane mode is marginally affected.[33,46] The softening of out-of-plane vibrating mode could have resulted from an increased electron density in the layer, which is consistent with the Raman spectra of n-type Fe:MoS$_2$ reported by Kang et al.[46] Moreover, as indicated by Iqbal et al.,[47] in-plane E$^1_{2g}$ mode is sensitive to strain, while the out-of-plane A$_{1g}$ mode is sensitive to doping; this is exactly reflected in Fig. 3(c), wherein $C_\parallel$ increases with the applied pressure (strain), while $C_\perp$ exhibits an essentially pressure-independent behavior. The compressive force ratio ($C_\perp / C_\parallel$) as a function of pressure is shown in Fig. S7 and the force constants' pressure derivatives for each pressure zones are listed in Table SIV. Figure S7 also suggests that the iron impurity in MoS$_2$ is an n-type dopant.

In summary, we have carried out high-pressure ADXRD and optical Raman scattering measurements on Fe:MoS$_2$ up to 19.7(1) and 24.8(2) GPa, respectively. The ADXRD and Raman results consistently reveal that the electronic phase transitions are similar to those of pristine MoS$_2$ but occur at significantly lower pressures. The discontinuities in pressure-dependence of micro-strain coincide with the changing rate in lattice compressions, suggesting that the combinational effects of local strain-induced lattice instability, the variations in interlayer van der Waals bonding associated with the shortened Fe-S bond, and in-gap states introduced by Fe-doping are responsible for the early onset of the electronic transitions. Raman peak splitting and phonon softening are observed at the same transition pressures, implying that the electronic transitions may also be closely related to the evolutions in the microstructure. Our findings provide a new approach of vdW engineering for manipulating the electronic and magnetic properties of the emergent family of two-dimensional diluted magnetic semiconductors.

See the supplementary material for additional information about cell parameters of multilayered Fe:MoS$_2$ with pressures (Table SI), pressure dependence of the d-spacings in three transition zones of multilayered Fe:MoS$_2$ at 300 K (Table SII), the mode frequencies vs the pressure and Grüneisen parameter (γ_i) of E$_{2g}(\Gamma)$ and A$_{1g}(\Gamma)$ modes in three zones (Table SIII), the compressional force constant of out-of-plane (C_b^c), in-plane (C_w^c), their pressure derivatives for respective zones (Table SIV), comparison of growth methods (Table SV), ICP-OES spectrum (Fig. S1), pressure dependence of the d-spacings (Fig. S2) and volume (Fig. S3) of multilayered Fe:MoS$_2$ in respective zones at 300 K, the $(2\omega_{hkl})^2\cos^2\theta_{hkl}$ vs $\sin^2\theta_{hkl}$ plot for multilayered Fe:MoS$_2$ at 8.6(1) GPa (Fig. S4), the deconvoluted Raman spectra of multilayered Fe:MoS$_2$ at ambient conditions (Fig. S5) and at 2.2(1) GPa (Fig. S6), ratio of compressive forces as a function of pressure (Fig. S7), the top view SEM images, EDX spectra and EDX spectroscopy mapping for (a) pristine MoS$_2$ and (b) Fe-doped MoS$_2$ (Fig. S8) and the side view SEM images, EDX spectra, and EDX spectroscopy mapping for (a) pristine MoS$_2$ and (b) Fe-doped MoS$_2$ (Fig. S9).

AUTHOR DECLARATIONS
Conflict of Interest

The authors have no conflicts to disclose.

Author Contributions

Chih-Ming Lin: Conceptualization (equal); Data curation (equal); Formal analysis (equal); Funding acquisition (equal); Investigation (equal); Methodology (equal); Writing – original draft (equal); Writing – review & editing (equal). **Der-Yuh Lin:** Data curation (equal); Investigation (equal); Methodology (equal). **Jenh-Yih Juang:** Conceptualization (equal); Formal analysis (equal); Investigation (equal); Methodology (equal); Writing – original draft (equal); Writing – review & editing (equal). **Tony Huang:** Data curation (equal); Investigation (equal); Software (equal). **Dong-Zhou Zhang:** Data curation (equal); Formal analysis (equal); Methodology (equal); Software (equal). **Yi-Jia Tsai:** Data curation (equal); Software (equal). **Sheng-Rui Jian:** Conceptualization (equal); Formal analysis (equal); Methodology (equal). **Joon-Seok Kim:** Conceptualization (equal); Data curation (equal); Formal analysis (equal); Investigation (equal); Writing – original draft (equal); Writing – review & editing (equal). **Jung-Fu Lin:** Data curation (equal); Investigation (equal); Methodology (equal).

DATA AVAILABILITY

The data that support the findings of this study are available from the corresponding authors upon reasonable request.

REFERENCES

[1] Y. P. Feng, L. Shen, M. Yang, A. Wang, M. Zeng, Q. Wu, S. Chintalapati, and C. R. Chang, WIREs Comput. Mol. Sci. **7**, e1313 (2017).

[2] E. C. Ahn, npj 2D Mater. Appl. **4**, 17 (2020).

[3] B. L. Cao, Z. M. Ye, L. Yang, L. Gou, and Z. G. Wang, Nanotechnology **32**(41), 412001 (2021).

[4] Q. H. Wang, K. Z. A. Kis, J. N. Coleman, and M. S. Strano, Nat. Nanotechnol. **7**, 699 (2012).

[5] B. Radisavljevic, A. Radenovic, J. Brivio, V. Giacometti, and A. Kis, Nat. Nanotechnol. **6**, 147 (2011).

[6] A. Kuc, N. Zibouche, and T. Heine, Phys. Rev. B **83**, 245213 (2011).

[7]S. Fu, K. Kang, K. Shayan, A. Yoshimura, S. Dadras, X. Wang, L. Zhang, S. Chen, N. Liu, A. Jindal, X. Li, A. N. Pasupathy, A. N. Vamivakas, V. Meunier, S. Strauf, and E. H. Yang, Nat. Commun. **11**, 2034 (2020).

[8]H. Li, M. Cheng, P. Wang, R. Du, L. Song, J. He, and J. Shi, Adv. Mater. **34**, 2200885 (2022).

[9]K. F. Mak, K. He, C. Lee, G. H. Lee, J. Hone, T. F. Heinz, and J. Shan, Nat. Mater. **12**, 207–211 (2013).

[10]A. Raja, A. Chaves, J. Yu, G. Arefe, H. M. Hill, A. F. Rigosi, T. C. Berkelbach, P. Nagler, C. Schüller, T. Korn, C. Nuckolls, J. Hone, L. E. Brus, T. F. Heinz, D. R. Reichman, and A. Chernikov, Nat. Commun. **8**, 15251 (2017).

[11]X. Hong, J. Kim, S. Shi, Y. Zhang, C. Jin, Y. Sun, S. Tongay, J. Wu, Y. Zhang, and F. Wang, Nat. Nanotechnol. **9**, 682–686 (2014).

[12]A. Weston, E. G. Castanon, V. Enaldiev, F. Ferreira, S. Bhattacharjee, S. Xu, H. Corte-León, Z. Wu, N. Clark, A. Summerfield, T. Hashimoto, Y. Gao, W. Wang, M. Hamer, H. Read, L. Fumagalli, A. V. Kretini, S. J. Haigh, O. Kazakova, A. K. Geim, V. I. Fal'ko, and R. Gorbachev, Nat. Nanotechnol. **17**, 390–395 (2022).

[13]J. S. Kim, N. Maity, M. Kim, S. Fu, R. Juneja, A. Singh, D. Akinwande, and J. F. Lin, ACS Appl. Mater. Interfaces **14**(41), 46841 (2022).

[14]L. Hromadová, R. Martoňák, and E. Tosatti, Phys. Rev. B **87**, 144105 (2013).

[15]S. Bhattacharyya and A. K. Singh, Phys. Rev. B **86**, 075454 (2012).

[16]C. Espejo, T. Rangel, A. H. Romero, X. Gonze, and G. M. Rignanese, Phys. Rev. B **87**, 245114 (2013).

[17]H. Guo, T. Yang, P. Tao, Y. Wang, and Z. Zhang, J. Appl. Phys. **113**, 013709 (2013).

[18]R. Aksoy, Y. Z. Ma, E. Selvi, M. C. Chyu, A. Ertas, and A. White, J. Phys. Chem. Solids **67**, 1914 (2006).

[19]A. P. Nayak, S. Bhattacharyya, J. Zhu, J. Liu, X. Wu, T. Pandey, C. Jin, A. K. Singh, D. Akinwande, and J. F. Lin, Nat. Commun. **5**, 3731 (2014).

[20]Z. H. Chi, X. M. Zhao, H. Zhang, A. F. Goncharov, S. S. Lobanov, T. Kagayama, M. Sakata, and X. J. Chen, Phys. Rev. Lett. **113**, 036802 (2014).

[21]J. S. Kim, R. Ahmad, T. Pandey, A. Rai, S. Feng, J. Yang, Z. Lin, M. Terrones, S. K. Banerjee, A. K. Singh, D. Akinwande, and J. F. Lin, 2D Mater. **5**(1), 015008 (2017).

[22]M. López-Suárez, I. Neri, and R. Rurali, J. Appl. Phys. **119**, 165105 (2016).

[23]X. Cheng, Y. Li, J. Shang, C. Hu, Y. Ren, M. Liu, and Z. Qi, Nano Res. **11**(2), 855 (2018).

[24]Q. Li, X. Zhao, L. Deng, Z. Shi, S. Liu, Q. Wei, L. Zhang, Y. Cheng, L. Zhang, H. Lu, W. Gao, W. Huang, C. W. Qiu, G. Xiang, S. J. Pennycook, Q. Xiong, K. P. Loh, and B. Peng, ACS Nano **14**, 4636 (2020).

[25]L. Pauling, J. Am. Chem. Soc. **54**, 3570 (1932).

[26]X. B. Yu, G. Y. Zhao, C. Liu, C. L. Wu, H. H. Huang, J. J. He, and N. Q. Zhang, Adv. Funct. Mater. **31**, 2103214 (2021).

[27]A. W. Webb, J. L. Feldman, E. F. Skelton, L. C. Towle, C. Y. Liu, and I. L. Spain, J. Phys. Chem. Solids **37**, 329 (1976).

[28]G. A. N. Connel, J. A. Wilson, and A. D. Yoppe, J. Phys. Chem. Solids **30**, 287 (1969).

[29]C. M. Lin, I. J. Hsu, S. C. Lin, Y. C. Chuang, W. T. Chen, Y. F. Liao, and J. Y. Juang, Sci. Rep. **8**, 1284 (2018).

[30]T. Schulz, T. Remmele, T. Markurt, M. Korytov, and M. Albrecht, J. Appl. Phys. **112**, 033106 (2012).

[31]B. Palosz, S. Stel'makh, E. Grzanka, S. Gierlotka, R. Pielaszek, S. Werner, and W. Palosz, J. Phys.: Condens. Matter **16**, S353 (2004).

[32]J. S. Kim, R. Juneja, N. P. Salke, W. Palosz, V. Swaminathan, S. Trivedi, A. K. Singh, D. Akinwande, and J. F. Lin, J. Appl. Phys. **123**, 115903 (2018).

[33]T. J. Wieting, Solid State Commun. **12**, 931 (1973).

[34]G. L. Frey, R. Tenne, M. J. Matthews, M. S. Dresselhaus, and G. Dresselhaus, Phys. Rev. B **60**, 2883 (1999).

[35]H. Li, Q. Zhang, C. C. Ray Yap, B. K. Tay, T. H. Tong Edwin, A. Olivier, and D. Baillargeat, Adv. Funct. Mater. **22**, 1385 (2012).

[36]K. Golasa, M. Grzeszczyk, P. Leszczynski, C. Faugeras, A. A. L. Nicolet, A. Wysmolek, M. Potemski, and A. Babinski, Appl. Phys. Lett. **104**, 092106 (2014).

[37]M. Placidi, M. Dimitrievska, V. Izquierdo-Roca, X. Fontané, A. Castellanos-Gomez, A. Pérez-Tomás, N. Mestres, M. Espindola-Rodriguez, S. López-Marino, M. Neuschitzer, V. Bermudez, A. Yaremko, and A. Pérez-Rodríguez, 2D Mater. **2**, 035006 (2015).

[38]C. S. Park, Y. Shon, J. Lee, and E. K. Kim, Solid State Commun. **306**, 113776 (2020).

[39]H. J. Conley, B. Wang, J. I. Ziegler, J. R. F. Haglund, S. T. Pantelides, and K. I. Bolotin, Nano Lett. **13**, 3626 (2013).

[40]C. Rice, R. Young, R. Zan, U. Bangert, D. Wolverson, T. Georgiou, R. Jalil, and K. S. Novoselov, Phys. Rev. B **87**, 081307 (2013).

[41]A. Bera, K. Pal, D. V. S. Muthu, S. Sen, P. Guptasarma, U. V. Waghmare, and A. K. Sood, Phys. Rev. Lett. **110**, 107401 (2013).

[42]C. M. Lin, D. S. Chuu, T. J. Yang, W. C. Chou, J. A. Xu, and E. Huang, Phys. Rev. B **55**, 13641 (1997).

[43]R. Mittal, R. P. Hermann, M. Angst, S. L. Chaplot, E. E. Alp, J. Zhao, W. Sturhahn, and F. Hatert, arXiv:0903.1550 [cond-mat.mtrl-sci] (2009).

[44]C. J. Hearn, J. Phys. C: Solid State Phys. **5**, 1317 (1972).

[45]S. Sugai, T. Ueda, and K. Murase, J. Phys. Colloques **42**, C6-320 (1981).

[46]K. Kang, S. Fu, K. Shayan, A. Yoshimura, S. Dadras, Y. Xiong, M. Fujisawa, M. Terrones, W. Zhang, S. Strauf, V. Meunier, A. N. Vamivakas, and E. H. Yang, Nanotechnology **32**(9), 095708 (2021).

[47]M. W. Iqbal, K. Shahzad, R. Akbar, and G. Hussain, Microelectron. Eng. **219**, 111152 (2020).